INFLUENCE FACTORS OF LAND SURFACE TEMPERATURE INVERSION USING THERMAL INFRARED HYPERSPECTRAL REMOTE SENSING SATELLITES DATA

Tinghao Liu [1]*, Zhen Li [1], Shaocong Liu [1], Xianfei Qiu [1]

[1] Institute of Remote Sensing Satellite, China Academy of Space Technology, Beijing 100094, China - dpimlth11@126.com

KEY WORDS: Land Surface Temperature, Land Surface Emissivity, Thermal Infrared, Hyperspectral, Influencing Factors.

ABSTRACT:

Land surface temperature (LST) is widely used in research fields such as numerical forecasting, global circulation models, and regional climate models. For the remote sensing data from satellites with thermal infrared detection capability, the land surface temperature (LST), land surface emissivity (LSE), and atmospheric influence are mixed together. Using different assumptions and approximations for the radiative transfer equations and surface emissivity, various LST algorithms have been proposed. Among these algorithms, the split-window (SW) algorithm is currently most widely used. Besides, with the rapid development of machine learning, new ideas have been emerged for quantitative remote sensing inversion. For a hyperspectral remote sensing satellite with over 20 thermal infrared channels, machine learning methods such as random forest and artificial neural network can be selected to build an integrated separation and inversion algorithm for LST and LSE.
In this paper, the influencing factors of LST inversion using thermal infrared hyperspectral satellites data is discussed, taking the SW algorithm and integrated machine learning algorithm as examples, and the contribution of these factors to the LST inversion error is analysed. We hope this paper could provide valuable reference for the design, index analysis and error calculation for remote sensing satellites with thermal infrared hyperspectral detection capability.

1. INTRODUCTION

Research on the use of infrared remote sensing satellites began in the early 1960s. In the decades since then, with the increasing number of satellite sensors with infrared detection capability, various applications have been developed for infrared remote sensing data.

Thermal infrared remote sensing data has a wide range of applications, such as land and earth science, fire detection, security monitoring, and land surface temperature inversion. Land surface temperature (LST), as a key parameter in many application fields, can provide spatiotemporal changes in the state of surface energy balance, and is widely used in research fields such as numerical forecasting, global circulation models, and regional climate models. Accurate land surface temperature can not only help to evaluate the assessment of surface energy, hydrological balance, thermal inertia and soil moisture, but also to obtain global surface temperatures and grasp their long-term variability.

For the remote sensing data from satellites with thermal infrared detection capability, the land surface temperature, land surface emissivity (LSE), and atmospheric influence are mixed together in the pupil radiance of the sensor. Using different assumptions and approximations for the radiative transfer equations and surface emissivity, various LST inversion algorithms have been proposed, such as single-channel algorithm, dual channel algorithm, split-window (SW) algorithm, multi-angle algorithm, Temperature and Emissivity Separation (TES) algorithm, and SW-TES algorithm.

Among these algorithms, the split-window (SW) algorithm is currently most widely used. This algorithm needs land surface emissivity of the detection area as a prior knowledge. The basic principle of the SW algorithm is to utilize the differences in atmospheric absorption (especially the difference in atmospheric water vapor absorption) between two channels within the atmospheric window, and to perform land surface temperature inversion by various combinations of brightness temperatures on these two channels. This method does not require any atmospheric profile information, and has high accuracy and fast calculation speed.

With the rapid development of machine learning, new ideas have been emerged for quantitative remote sensing inversion. Machine learning can directly describe the complex nonlinear relationship, so as to build the relationship between the satellite pupil radiance, land surface temperature and emissivity, which can provide great convenience for the separation and retrieval of LST and LSE. Thus, for a hyperspectral remote sensing satellite with over 20 thermal infrared channels, machine learning methods such as random forest and artificial neural network can be selected to build an integrated separation and inversion algorithm for LST and LSE. Using the much abundant data of hyperspectral remote sensing data, without the need of prior knowledge of LSE or atmospheric profile, this algorithm can eliminate the influence of these two factors, and achieve accurate inversion of LST.

In this paper, the influencing factors of LST inversion using thermal infrared hyperspectral satellites data is discussed, taking the SW algorithm and integrated machine learning algorithm as examples, and the contribution of these factors to the LST inversion error is analysed. We hope this paper could provide valuable reference for the design, index analysis and error calculation for remote sensing satellites with thermal infrared hyperspectral detection capability.

https://doi.org/10.5194/isprs-archives-XLVIII-1-W2-2023-1431-2023

2. LAND SURFACE TEMPERATURE INVERSION ALGORITHMS

2.1 Principle of Thermal Infrared Radiation Transmission

In the thermal infrared band, the solar radiation energy could be ignored. Assuming that the land surface is Lambert body, the thermal infrared radiation transfer equation can be expressed as (Becker and Li, 1990):

$$L_i(\theta) = \tau_i(\theta)L_G(\theta) + L_i^{\uparrow}(\theta) \quad (1)$$

where, θ is the observation zenith of the sensor,
$\tau_i(\theta)$ is the atmospheric transmittance of Channel i in the direction from the target to the sensor,
$L^{\uparrow}{}_i(\theta)$ is the upward atmosphere thermal radiation of Channel i,
$L_G(\theta)$ is the surface thermal radiation observed on the ground in Channel i, which can be expressed as:

$$L_G(\theta) = \varepsilon_i(\theta)B_i(T_s) + (1-\varepsilon_i(\theta))L_i^{\downarrow} \quad (2)$$

where, $\varepsilon_i(\theta)$ is the angular radiance of Channel and angle θ,
B_i is the Plonk function,
T_s is the land surface temperature (LST),
$L_i^{\downarrow}$ is downward atmosphere thermal radiation of Channel i,

2.2 Land Surface Temperature Inversion Algorithms

The key of LST inversion is to complete the decoupling of earth atmosphere parameters and eliminate the influence of LST, LSE and the atmosphere. Different algorithms for land surface temperature inversion have been developed. Below is an introduction to the typical surface temperature inversion algorithms.

2.2.1 Single-channel algorithm: This algorithm uses the single channel data received by satellites at the atmospheric window to correct the atmospheric attenuation and emission using the atmospheric transmittance/radiation program in which the atmospheric profile data is needed as an input (Ottlé and Vidal-Madjar,1992; Jiménez-Muñoz and Sobrino, 2005; Zhang and Li, 2022). Then, under the condition that LSE is already known, the LST can be obtained by inverse calculation of Equation (1) and (2). It should be noted that the this algorithm is useful provided that the LSE and atmospheric profile are known, which is difficult to obtain in practical applications.

2.2.2 Split-window algorithm: This algorithm is currently the most widely used algorithm for LST inversion. The basic principle is to utilize the differences in atmospheric absorption (especially the difference in atmospheric water vapor absorption) between two channels within the atmospheric window, and to perform land surface temperature inversion by various combinations of brightness temperatures on these two channels. This method does not require any atmospheric profile information, and has high accuracy and fast calculation speed, thus has been widely applied to different thermal infrared satellites, such as AVHRR (Becker and Li, 1990), MODIS (Wan and Dozier, 1996), and GOES (Sun and Pinker, 2003). However, all split-window algorithms have been developed on the assumption that the LSE is already known so far.

2.2.3 Temperature emissivity separation algorithm: This algorithm (TES) was proposed by Gillespie (1998) for ASTER data. TES algorithm absorbs the advantages of Normalized Emissivity Method (NEM, Gillespie, 1996) , Spectral Ratio Method (SR) and Maximum-Minimum Apparent Emissivity Difference method (MMD, Matsunaga, 1994) , and makes some improvements. This method is more suitable for ground objects with large spectral differences in emissivity (such as rock and soil) . However, the inversion error is relatively large in areas where the spectral difference of emissivity is small, such as vegetation, water, ice and snow, and in humid and hot atmosphere. Hulley and Hook (2011) developed a TES algorithm using three MODIS thermal infrared bands (bands 29,31 and 32) .

2.2.4 Integrated machine learning algorithm: With the rapid development of machine learning, new ideas have been emerged for quantitative remote sensing inversion. Machine learning can directly describe the complex nonlinear relationship, so as to build the relationship between the satellite pupil radiance, LST and LSE, which provides great convenience for the separation and retrieval of LST and LSE. Thus, for a hyperspectral remote sensing satellite with over 20 thermal infrared channels, machine learning methods such as random forest and artificial neural network can be selected to build an integrated separation and inversion algorithm for LST and LSE. Using the much abundant data of hyperspectral remote sensing data, without the need of prior knowledge of LSE or atmospheric profile, this algorithm can eliminate the influence of these two factors, and achieve accurate inversion of LST.

2.2.5 Other inversion algorithms: Limited by the length of this article, other inversion algorithms, such as Multi-angle algorithm (Chedin et al., 1982; Sòria and Sobrino,2007), Day / night algorithm (Wan and Li, 1997, 2011), SW-TES algorithm (Zheng et al., 2019), et al, will not be explained in detail here.

2.2.6 Inversion algorithms comparison: Table 1 summarizes the applicability, advantages, and disadvantages of commonly used LST inversion algorithms, including Single-channel algorithm, Split-window algorithm, Temperature emissivity separation algorithm, Integrated machine learning algorithm, Multi-angle algorithm, Dual channel algorithm, and SW-TES algorithm.

3. INFLUENCING FACTORS TO LST INVERSION ERROR OF SPLIT-WINDOW ALGORITHM

3.1 Optimal band combination

The basis of the Split-Window algorithm is the different absorption effects between two channels within the atmospheric window. These channels usually refers to the two thermal infrared bands between the 10-12.5 μm atmospheric window, but it can also include the bands between 8-9.5 μ m. The split window algorithm used in this article is as follows:

$$LST = b_0 + (b_1 + b_2\frac{1-\varepsilon}{\varepsilon} + b_3\frac{\Delta\varepsilon}{\varepsilon^2})\frac{T_i+T_j}{2} + (b_4 + b_5\frac{1-\varepsilon}{\varepsilon} + b_6\frac{\Delta\varepsilon}{\varepsilon^2})\frac{T_i-T_j}{2} + b_7(T_i-T_j)^2 \quad (3)$$

where, T_i and T_j are the top atmospheric brightness temperatures of the two split window bands,
ε is the average emissivity of two bands, $\varepsilon=0.5(\varepsilon_i+\varepsilon_j)$,
b_0~b_7 are the SW coefficients that need to be determined from simulated data

Algorithms	Sensor requirement	External input needed	Advantages	Disadvantages	Accuracy
Single-channel	Only 1 thermal infrared channel	columnar water vapor (CWV) or atmospheric profile, LSE	Only one channel needed	Atmospheric correction needed, low accuracy when CWV is high	1.5-2.5K (CWV $<3g/cm^2$)
Split-window	2 channels in 10~13μm	LSE	Simple algorithm, fast speed, automatic atmospheric correction	Very sensitive to LSE	1K(Dense vegetation and water bodies); 2~3K (others)
Temperature emissivity separation	3~5 channels in 8~12μm	Atmospheric profile	LST and LSE inversed simultaneously	Atmospheric radiation transfer models needed for atmospheric correction, slow speed	1.5K theoretically
Integrated machine learning	Hyperspectral thermal infrared data	No need	LST and LSE inversed simultaneously, no external input required	Large number of infrared channels required	2K theoretically
Multi-angle	Observations from two or more angles	LSE	Automatic atmospheric correction	Difficult to obtain multi angle observation data, only applicable to uniform surfaces	1.5K theoretically
Dual channel	A thermal infrared and a mid infrared channel	LSE	Suitable for data with both mid infrared and thermal infrared	During the day, mid infrared can bring some errors	Day: 3K Night: 2K
SW-TES	5 specific channels (8.6, 9.0, 10.4, 11.3, and 12.5 μm)	No need	LST and LSE of 3 channels inversed simultaneously, no external input required	High requirement for sensor, no space sensor could meet yet	Day: 3K Night: 2K

Table 1. **Applicability, advantages, and disadvantages of commonly used LST inversion algorithms.**

This algorithm is the official LST product of MODIS. The main advantages of this algorithm are: 1) it is a physics based algorithm, as it applies the radiation transfer equation to two different bands and minimizes experience; 2) It takes into account the effects of observation angle, LSE and atmospheric water vapor; 3) The accuracy is high and relatively simple, requiring minimal computational time.

Different band combinations can be selected in the range of 8-10.5μm and 8-12.5μm. In order to obtain the performance of different configurations, we constructed a complete simulation dataset. The simulated sensor radiance (or onboard brightness temperature) is calculated using formula (3) combined with surface parameters (LST or LSE) and atmospheric parameters. The atmospheric parameters used are calculated using the atmospheric profile database Thermodynamic Initial Guess Retrieval (TIGR) profile library (including information on altitude, pressure, temperature, and relative humidity of atmospheric profiles), and the atmospheric radiation transfer model MODTRAN. The LSE is extracted from ASTER spectral library (ASTERlib) and UCSB spectral library (Baldridge, Hook, Grove, and Rivera, 2009). The spectral response function of the the sensor (Jiménez-Muñoz & Sobrino, 2003) is simulated by the following formula:

$$f(\lambda)=\begin{cases}\dfrac{\lambda}{FWHM}+\left(1-\dfrac{\lambda_0}{FWHM}\right) & \lambda_0-FWHM<\lambda<\lambda_0-\dfrac{FWHM}{2}\\ \exp\left[-\dfrac{(\lambda-\lambda_0)^2}{2\sigma^2}\right] & \lambda_0-\dfrac{FWHM}{2}<\lambda<\lambda_0+\dfrac{FWHM}{2}\\ -\dfrac{\lambda}{FWHM}+\left(1+\dfrac{\lambda_0}{FWHM}\right) & \lambda_0+\dfrac{FWHM}{2}<\lambda<\lambda_0+FWHM\end{cases} \quad (4)$$

where, FWHM is the half width of the spectral channel.
Firstly, the band combinations within the detection range of 8~10.5 μm range are analyzed, with a central wavelength range of 8.0-9.5μm and 9.0-10.5 μm, respectively. The step size is 0.1μm. Root-mean-square deviation (RMSE) is used to select the best band combination. Then the the band combinations within the 8~12.5μm range are analyzed, with a central wavelength range of 9.5-11.0μm and 10.5-12.0μm, respectively,.

①FWHM1=0.25μm and FWHM2=0.25μm in 8~10.5μm: the inversion error corresponding to 241 band configurations is shown in Figure 1(a), indicating the optimal central wavelength ranges is 8.0~8.1μm, and 9.0-9.1μm, respectively, with a theoretical inversion error of the SW algorithm as 1.02K.

②FWHM1=0.5μm and FWHM2=0.5μm in 8~10.5μm : the inversion error is shown in Figure 1(b), indicating the optimal central wavelength ranges is 8.0~8.1μm, and 9.0-9.1μm, respectively, with a theoretical inversion error of the SW algorithm as 1.12K.

③FWHM1=0.25μm and FWHM2=0.25μm in 8~12.5μm : the inversion error is shown in Figure 1(c), indicating the optimal central wavelength ranges is 10.4~10.8μm, and 11.4~11.9μm, respectively, with a theoretical inversion error of the SW algorithm as 0.68K.

④FWHM1=0.5μm and FWHM2=0.5μm in 8~12.5μm: the inversion error is shown in Figure 1(d), indicating the optimal central wavelength ranges is 10.4~10.8μm, and 11.6~11.9μm, respectively, with a theoretical inversion error of the SW algorithm as about 0.68K.

⑤FWHM1=0.7μm and FWHM2=1.0μm in 8~12.5μm : the inversion error is shown in Figure 1(e), indicating the optimal central wavelength is 10.4~10.8μm, and 11.6~11.9μm,

respectively, with a theoretical inversion error of the SW algorithm as about 0.76K.

From the different FWHM within the above two band ranges, it can be seen the theoretical inversion errors of the SW algorithm are similar when the FWHM is 0.25μm and 0.5 μm, but increase with higher FWHM. In order to meet the needs of different sensors, the optimal band combinations within 8~10.5 μm and 8~12.5 μm range are summarized in Table 2.

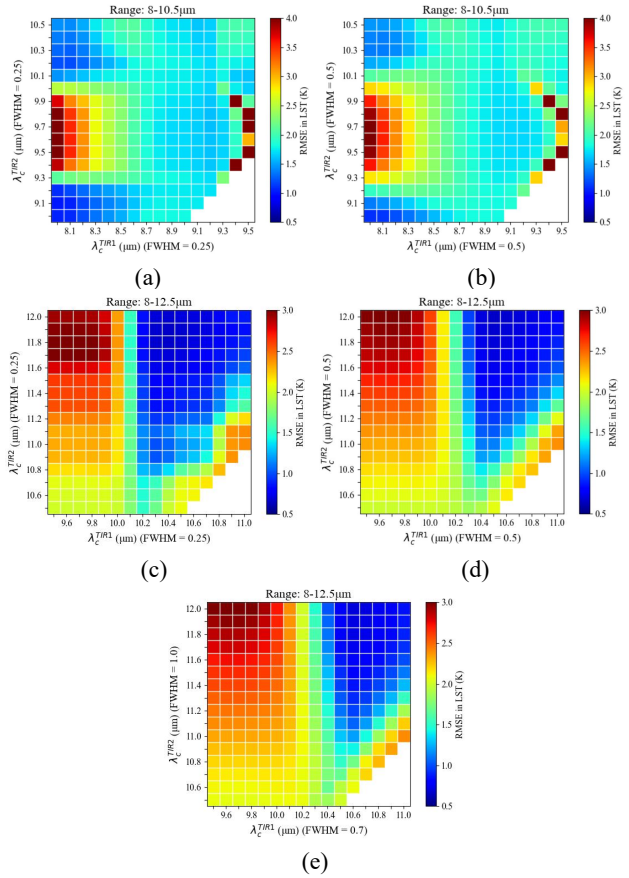

Figure 1. Error values corresponding to band combinations.
(a)FWHM1=0.25μm and FWHM2=0.25μm in 8~10.5μm;
(b)FWHM1=0.25μm and FWHM2=0.25μm in 8~10.5μm;
(c)FWHM1=0.25μm and FWHM2=0.25μm in 8~12.5μm;
(d)FWHM1=0.5μm and FWHM2=0.5μm in 8~12.5μm;
(e)FWHM1=0.7μm and FWHM2=1.0μm in 8~12.5μm

Detection range	Band 1 (μm)	FWHM 1 (μm)	Band 2 (μm)	FWHM2 (μm)
8~10.5μm	8.1±0.1	0.5±0.1	9.0±0.1	0.5±0.1
8~12.5μm	10.6±0.2	0.5±0.15	11.9±0.2	0.5±0.15

Table 2. Optimal band combinations of SW algorithm.

3.2 Inversion error analysis

The factors that affect the accuracy of LST inversion using SW algorithm include the algorithm error itself, the noise equivalent temperature difference (NEΔT) of the sensor, LSE uncertainty, and absolute calibration accuracy on inversion accuracy. The final error calculation formula of the SW algorithm is as follows:

$$e(LST) = \sqrt{\delta(alg)^2 + \delta(NE\Delta T)^2 + \delta(\varepsilon)^2 + \delta(cal)^2} \quad (5)$$

where, $\delta(alg)$ is the error of the split window algorithm itself, $\delta(NE\Delta T)$, $\delta(\varepsilon)$, $\delta(cal)$ are the error caused by NEΔT, LSE, and absolute calibration accuracy, respectively.

Taking the SW band of 8.1/9.0 μm and 10.6/11.9 μm with FWHM=0.5μm as the window channel, the influencing factors are elaborated in 3.2.1~3.2.3.

3.2.1 NEΔT: The impact on the inversion error of SW algorithm of NEΔT can be expressed as :

$$\delta_{NE\Delta T} = \sqrt{(\frac{\partial T_s}{\partial T_i})e^2(T_i) + (\frac{\partial T_s}{\partial T_j})e^2(T_j)} \quad (6)$$

Figure 2 shows the increase of LST error when NEΔT increases, when other items $\delta(\varepsilon)$, $\delta(W)$, $\delta(cal)$ remains constant. In this simulation scenario, The relationship between NEΔT and $\delta(NE\Delta T)$ is linear, with almost no y intercept, and the slope is around 3, indicating that LST error caused by NEΔT is approximately three times value of NEΔT. For a sensor with NEΔT of 0.02K, the NEΔT caused error $\delta(NE\Delta T)$ is about 0.06K.

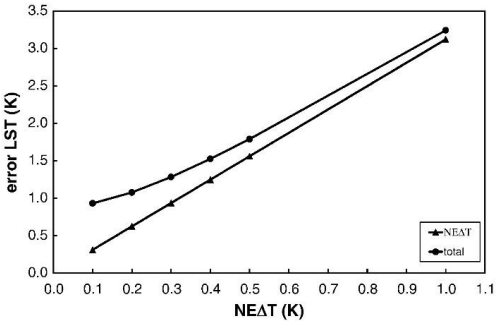

Figure 2. LST error caused by NEΔT

3.2.2 Absolute calibration accuracy: The absolute calibration accuracy can be directly applied to the inversion error calculation. For the application seeking high inversion accuracy (less than 1.5 K) , the absolute calibration accuracy should be be ensured to better than 1K.

3.2.3 LSE: From Formula (3), it can be seen that the uncertainty of LSE error is mainly reflected in $(1-\varepsilon)/\varepsilon$ and $\Delta\varepsilon/\varepsilon^2$. Their coefficients can be expressed as:

$$\alpha = b_2\frac{T_i+T_j}{2} + b_5\frac{T_i-T_j}{2} \quad (7)$$

$$\beta = b_3\frac{T_i+T_j}{2} + b_6\frac{T_i-T_j}{2} \quad (8)$$

Thus, the influence of LSE error on LST inversion can be expressed as:

$$\delta(\varepsilon) = \sqrt{\alpha^2\delta(\frac{1-\varepsilon}{\varepsilon})^2 + \beta^2\delta(\frac{\Delta\varepsilon}{\varepsilon^2})^2} \quad (9)$$

Using the simulated data set, the α and β in Formula (9) can be calculated, and the LST inversion error caused by LSE error can be estimated.

The spectra of 119 natural samples are selected to build the natural LSE library, which includes spectra of vegetation, water, ice, snow, rock, sand, and soil, as shown in Figure 3(a).At the same time, to simulate some unnatural objects, especially some artificial objects, a low LSE library with an average emissivity below 0.2 was constructed, as shown in Figure 3(b).

The coefficients and errors of the SW algorithm simulated by using the natural surface emissivity library and the low emisssivity library are shown in Table 3.

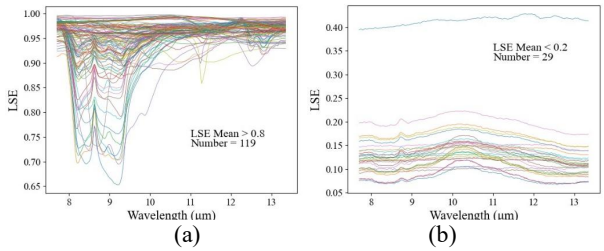

(a) (b)

Figure 3. Natural Emissivity samples(a) and low Emissivity samples(b) used in SW algorithm simulation

Library	Natural library		Natural &Low library	
range(μm)	8~10.5	8~12.5	8~10.5	8~12.5
b_0	1.591	-8.055	-48.517	-4.039
b_1	0.994	1.032	1.208	1.025
b_2	0.127	0.121	0.014	0.027
b_3	0.088	-0.322	-0.004	-0.016
b_4	-2.113	4.397	0.455	1.962
b_5	-1.276	2.97	-0.233	0.268
b_6	-0.914	-1.082	0.082	0.235
b_7	0.015	0.123	0.038	0.031
RMSE(K)	1.129	0.699	4.966	6.903

Table 3. SW Coefficient and algorithm error.

THe LST inversion error of natural samples is simulated. The error ranges of LSE within the range of 8~10.5μm and 8~12.5μm are 0.03-0.06 and 0.005-0.02 and the step sizes are 0.01 and 0.005, respectively. The analysis results are as follows.

Range (μm)	LSE error	Min (K)	Max (K)	Average (K)	RMS (K)
8-10.5	0.030	0.738	1.976	1.299	0.238
	0.040	0.984	2.635	1.732	0.317
	0.050	1.230	3.294	2.165	0.396
	0.060	1.476	3.952	2.598	0.475
8-12.5	0.005	0.358	0.598	0.461	0.053
	0.010	0.716	1.196	0.921	0.106
	0.015	1.074	1.794	1.382	0.159
	0.020	1.432	2.391	1.842	0.212

(a)

Range (μm)	LSE error	Min (K)	Max (K)	Average (K)	RMS (K)
8-10.5	0.030	0.007	0.220	0.112	0.046
	0.040	0.009	0.294	0.149	0.061
	0.050	0.012	0.367	0.187	0.076
	0.060	0.014	0.440	0.224	0.092
8-12.5	0.005	0.028	0.057	0.041	0.005
	0.010	0.055	0.114	0.081	0.011
	0.015	0.083	0.172	0.122	0.016
	0.020	0.111	0.229	0.163	0.021

(b)

Table 4. LST inversion error caused by $\delta(\varepsilon)$. (a)natural library; (b)natural & low emissivity library

3.2.3 Summary: Suppose the emissivity error of 8~10.5μm is 0.05 and that of 8~12.5μm is 0.015, the absolute calibration accuracy is 1K, the NEΔT of the sensor is 0.02K, the overall inversion error of LST is shown in Tabel 5.

	Natural library		Natural &Low library	
Band 1(μm)	8.1	10.6	8.1	10.6
Band 2(μm)	9.0	11.9	9.0	11.9
$\delta(alg)$(K)	1.129	0.699	4.966	6.903
$\delta(\varepsilon)$(K)	2.165	1.382	0.187	0.122
$\delta(NE\Delta T)$(K)	0.06	0.06	0.06	0.06
$\delta(cal)$(K)	1	1	1	1
$e(LST)$ (K)	2.64	1.84	5.07	6.97

Table 5. Overall error analysis results of SW algorithm.

It can be seen that for natural objects, the error of 8~10.5μm is significantly higher than that of 8~12.5μm. The main source is LSE, because the emissivity fluctuates more between 8.1 and 9.0μm, which may cause greater error when estimating LSE. After adding low emissivity samples, the SW algorithm itself is difficult to achieve high accuracy, and the inversion error is rather high for both detection ranges, thus the SW algorithm is no longer applicable then.

4. INFLUENCING FACTORS TO LST INVERSION ERROR OF INTEGRATED MACHINE LEARNING ALGORITHM

For thermal infrared hyperspectral remote sensing data, there are more channels available for LST inversion. We selected two thermal infrared spectral bands, 8-10.5μm and 8-12.5μm, with a channel interval of 0.1 μm, thus 26 channels and 47 channels are obtained respectively to analyze the inversion error of LST. Based on the previous research experience and the characteristics of machine learning methods, we chose two machine learning methods for LST inversion, Random Forest (RF) and Artificial Neural Network (ANN), which both support the training of multiple output models and have similar research experience.

4.1 Construction of Datasets

To comprehensively consider the typical situation of the global atmosphere, 946 atmospheric profile data are selected using the TIGR database. To avoid excessive distribution of atmospheric profile at low water vapor content, we randomly select a certain number of atmospheric profiles within each water vapor content interval based on atmospheric water vapor content. Based on the selected atmospheric profiles, we use MODTRAN to further calculate the corresponding atmospheric transmittance and atmospheric upward and downward radiation.

For LSE spectrum, 383 emission spectra of rock, soil, artificial surface, vegetation and water are selected. In order to ensure that the sample set can cover a variety of ground object types of emissivity spectrum, we have further screened the emissivity spectrum set. A total of 100 emissivity spectra of typical landforms were selected, including 51 rock emissivity spectra, 30 soil emissivity spectra, 8 water emissivity spectra, 4 vegetation emissivity spectra, and 5 man-made surface emissivity spectra.

The disturbance settings of the surface temperature are as shown in Figure 4: based on the atmospheric bottom temperature, with a step size of 3K, perturb up and down 5 times.

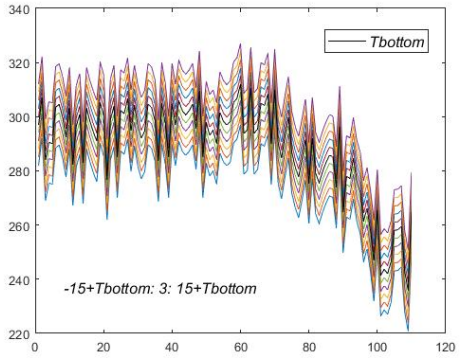

Figure 4. **Surface temperature dataset**

For spectral response function of the hyperspectral sensor, The central wavelengths of the two regions are generated with 0.1μm as the channel interval. Integrating the simulated data into the channel response, the final channel simulation data are obtained

4.2 Inversion results based on Random Forest algorithm

Random Forest algorithm has two most important super parameters, the maximum number of the decision tree, N-estimators, and the maximum number of features that can be selected when dividing attributes, Max-features. After debugging, the N-estimators is set as 200 and the Max-features is set as 20.

First the algorithm model inversion results is simulated. Then Then we add two kinds of noises to the data: NEΔT of 0.09K, and absolute radiometric calibration error of 1K, to verify the sensitivity of the random forest model to different noises. Both types of errors are Gaussian white noise and are added 50 times randomly.

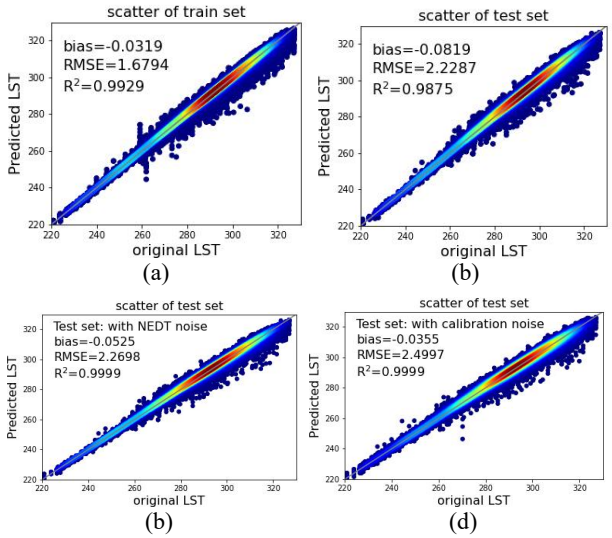

Figure 5. Inversion results of RF algorithm of 8~10.5μm. (a)training set; (b)test set; (c)test set with NEΔT noise; (d)test set with calibration noise

As shown Table 6 (a) and Figure 5, the inversion LST error of train set and test set are 1.68K and 2.23K, respectively. When the detection spectrum is extended to 12.5μm, the RMSE of temperature inversion can be reduced by about 1K. The inversion RMSE is not sensitive to NEΔT noise, but will significantly increase with the intervention of absolute radiometric calibration error.

Range(μm)	8-10.5		8-12.5	
Data set	Train set	Test set	Train set	Test set
w/o noise	1.68	2.23	0.90	1.20
w/ NEΔT	1.90	2.27	1.00	1.22
w/ Calibration	2.41	2.50	1.66	1.67
w/NEΔT& calibration	2.45	2.53	1.67	1.71

(a) RF algorithm

Range(μm)	8-10.5		8-12.5	
Data set	Train set	Test set	Train set	Test set
w/o noise	3.42	3.44	3.00	3.00
w/ NEΔT	3.48	3.49	3.01	3.01
w/ Calibration	3.61	3.63	3.17	3.17
w/NEΔT& calibration	3.67	3.68	3.18	3.18

(b) ANN algorithm

Table 6. **Inversion error of Integrated machine learning algorithms.** (a)RF algorithm; (b)ANN algorithm.

4.3 Inversion results based on Artificial Neural Network algorithm

It is generally considered that the three-layer ANN model is sufficient enough for the application of remote sensing to the inversion of surface radiation, and the neural network model with two hidden layers has better results for some extreme cases and discontinuities of the model. Therefore, we trained the MLP network model with two hidden layers, with the number of nodes in layer 1 and Layer 2 set to 100 and 80, respectively.

The simulated results is listed in Table 6(b).The inversion precision of ANN model is 3.7 K for LST at 8-10.5 μm, and 3.2K at 8-12.5 μm range. It can be seen that the LST inversion accuracy of ANN model is much lower than that of RF model.

5. CONCLUSION

This paper takes the SW algorithm and integrated machine learning algorithm as examples to analyze the influencing factors of LST inversion using thermal infrared hyperspectral remote sensing data.

Firstly, typical LST inversion methods are introduced and their applicability, advantages, and disadvantages are compared.

Subsequently, the factors affecting the inversion accuracy of the SW algorithm that requires two channels are analyzed. From the simulation results, the LST inversion effect of the two channels from 8 to 12.5μm is significantly better than that of 8 to 10.5μm. After the SW band is selected, the LSE error, absolute radiometric calibration error and algorithm error will have a greater impact on the overall inversion accuracy. Specifically, when conducting artificial ground object detection whose LSE is low, this algorithm is no longer applicable.

Next, the influencing factors of integrated machine learning algorithms are analyzed. This algorithm does not require additional input, making it more suitable for hyperspectral remote sensing applications with multiple spectral bands. The inversion results were evaluated by constructing a dataset and adding disturbances. The application of Random Rorest algorithm performs better, and the construction accuracy of data

sets and absolute radiometric calibration error have a great impact on the inversion accuracy.

In summary, in order to achieve good LST inversion results, the detection spectrum should be extended to above 12.5μm, and precise absolute radiometric calibration should be carried out. When observing natural features, the SW algorithm is applicable. For artificial ground objects, integrated detection can achieve better results.

REFERENCES

Becker F, Li Z L. (1990). Temperature-independent spectral indices in thermal infrared bands. *Remote Sensing of Environment*, 32(1), 17-33.

Ottlé C, Vidal-Madjar D. (1992). Estimation of land surface temperature with noaa9 data. *Remote Sensing of Environment,* 40(1), 27-41.

Sobrino J. A, Jiméne-Muñoz J.C. (2005). Land surface temperature retrieval from thermal infrared data: an assessment in the context of the surface processes and ecosystem changes through response analysis (spectra) mission. *Journal of Geophysical Research Atmospheres*, 110.

Zhang Q, Li D. C, et al. (2022). Quality validation of HJ-1B satellite land surface temperature products based on DTW. *Chinese Space Science and Technology*, 2022, 42 (3): 93-104 (in Chinese).

Becker F, Li Z.L. (1995). Surface temperature and emissivity at various scales: definition, measurement and related problems. *Remote Sensing Reviews*.

Wan Z, Dozier J. (1996). A generalized split-window algorithm for retrieving land-surface temperature from space. *IEEE Transactions on Geoscience & Remote Sensing*, 34(4), 892-905.

Sun D, Pinker R.T.(2003). Estimation of land surface temperature from geostationary operational environmental satellite (GOES-8). *Journal of Geophysical Research Atmospheres*, 108(D11).

Gillespie A, Rokugawa S, et al. (1998). A temperature and emissivity separation algorithm for advanced spaceborne thermal emission. *IEEE Transactions on Geoscience & Remote Sensing*, 36(4): 1113-1126.

Gillespie A.R. (1996). Temperature/emissivity separation algorithm theoretical basis document, version 2.4. Maryland, USA: NASA/GSFC: 1-64.

Matsunaga, T. A. (1994). A temperature-emissivity separation method using an empirical relationship between the mean, the maximum, and the minimum of the thermal infrared emissivity spectrum. *Journal of the Remote Sensing Society of Japan*, 14(2), 230-241.

Hulley G C, Hook S J (2011). Generating consistent land surface temperature and emissivity products between aster and modis data for earth science research. *IEEE Transactions on Geoscience and Remote Sensing*, 49(4), 1304-1315.

Chedin, A., Scott, N. A., and Berroir, A. (1982). A single-channel, double-viewing angle method for sea surface temperature determination from coincident Meteosat and TIROS-N radiometric measurements. *Journal of Applied Meteorology and Climatology*, 21(4), 613-618.

Sòria, G., and Sobrino, J. A. (2007). ENVISAT/AATSR derived land surface temperature over a heterogeneous region. *Remote Sensing of Environment*, 111(4), 409-422.

Wan, Z., and Li, Z. L. (1997). A physics-based algorithm for retrieving land-surface emissivity and temperature from EOS/MODIS data. *IEEE Transactions on Geoscience and Remote Sensing*, 35(4), 980-996.

Wan Z., and Li Z. L. . (2011). MODIS land surface temperature and emissivity. Taylor & Francis, Inc..

Zheng, X., Li, Z. L., Nerry, F., & Zhang, X. (2019). A new thermal infrared channel configuration for accurate land surface temperature retrieval from satellite data. *Remote Sensing of Environment*, 231, 111216.

Baldridge, A. M. , Hook, S. J. , Grove, C. I. , and Rivera, G. . (2009). The ASTER spectral library version 2.0. *Remote Sensing of Environment*, 113(4), 711-715.

Jiménez-Muñoz and Juan, C. (2003). A generalized single-channel method for retrieving land surface temperature from remote sensing data. *Journal of Geophysical Research Atmospheres*, 108(D22).